THE ASTROPHYSICAL JOURNAL, 398:621–631, 1992 October 20

MAPPING AG CARINAE: LONG-SLIT SPECTROSCOPY AND CORONOGRAPHIC IMAGING OF THE NEBULA AND JET[1]

ANTONELLA NOTA,[2,3] CLAUS LEITHERER,[2,3] MARK CLAMPIN,[4] PERRY GREENFIELD,[2] AND DAVID A. GOLIMOWSKI[4]

Received 1991 December 26; accepted 1992 April 24

ABSTRACT

New high-resolution images of the nebula around the luminous blue variable AG Carinae have been obtained with the Johns Hopkins Adaptive Optics Coronograph at the Swope 40 inch (1 m) telescope, Las Campanas, in the light of Hα + [N II] and in a narrow *V* continuum. The images confirm the presence of highly axisymmetric features in AG Carinae's circumstellar environment. In addition, we present new, high signal-to-noise ratio long-slit spectroscopic data, in the spectral range (6363–7254 Å), spatial resolution 0.″89 pixel^{-1}, and spectral resolution 40 km s^{-1}, with full spatial coverage of the nebula. Radial velocity maps of the nebula have been obtained in the Hα and [N II] lines and have been compared to the images to constrain the geometry of the system. The radial velocity data are consistent with a hollow, expanding shell ($v_{exp} \simeq 70$ km s^{-1}) but also show noticeable deviations from spherical symmetry. Possible interpretations are examined, such as the presence of an equatorial disk due to stellar rotation or, possibly, to a close, undetected companion, the presence of a magnetic field sufficiently strong to drive the wind, or density and pressure gradients in the local interstellar environment.

Subject headings: ISM: jets and outflows — stars: individual (AG Carinae) — stars: mass loss

1. INTRODUCTION

AG Carinae (=HD 94910 = CoD −59°3430 = CPD −59°2860) is a well-established variable star. Its photometric variability was first described by Wood (1914). The extraordinary nature of the star AG Carinae was recognized by Cannon (1916) who noted the presence of P Cygni lines in the stellar spectrum. Due to the strong stellar line emission, especially in Hα, AG Carinae has been detected in several surveys of Galactic emission-line objects. It is listed as MWC 216 (Merrill & Burwell 1933), M3-181 (Münch & Morgan 1953), and He 3-528 (Henize 1976).

AG Car has a plethora of photometric observations. Nearly continuous monitoring of the visual magnitude has been done from the beginning of the 20th century until the 1980s (see, e.g., Greenstein 1938, Mayall 1969, Bond & Landolt 1970, Wisse & Wisse 1971, Stahl 1986). AG Car displays quasi-periodic light variations between 7th and 9th mag on a time scale of about 10 yr. Superposed on these large-scale variabilities are smaller (~0.5 mag), erratic variations.

Caputo & Viotti (1970) performed a detailed study of the optical spectrum of AG Car and its variation with time. They found that the excitation and ionization conditions in the atmosphere change in a way to mimic equivalent spectral types from A1 I to B0 I over a time span of 10 yr. This study and subsequent works in the optical and ultraviolet spectral regions by Viotti (1971), Johnson (1980, 1982), Wolf & Stahl (1982), and Stahl (1986) suggest that AG Car is a massive, evolved star undergoing a very high rate of stellar mass loss. Based on its photometric and spectroscopic characteristics AG Car has been classified as a luminous blue variable (LBV; Humphreys 1989). LBVs are a class of stars which are believed to represent a short-lived (10^4–10^5 yr) phase during the evolution of a massive star where a significant amount of mass is ejected (Maeder 1989).

AG Car is one of the cornerstones for our understanding of the LBV phenomenon. Viotti et al. (1984) found that an increase in brightness at visual wavelengths is accompanied by a corresponding decrease in the ultraviolet so that the total bolometric luminosity of AG Car remains constant despite the large light variations. Photometric observations of AG Car in the infrared (Whitelock et al. 1983) also support such a scenario. Qualitatively similar results have been obtained for other LBVs like R127 (Stahl et al. 1983) or S Doradus (Leitherer et al. 1985). However, S Doradus and R127 (and other *extragalactic* LBVs) have photometric and spectroscopic histories which are less well documented. Therefore the *Galactic* LBV AG Car provides by far the best observational constraints for the suggestion that LBVs vary with the bolometric luminosity remaining constant.

Thackeray (1950) discovered an elliptical nebulosity of 39″ × 30″ in outer diameter around AG Carinae. The nebula, which has a distinct shell-like appearance on low-resolution images, was later included as 289 − 0°1 in the catalog of planetary nebulae by Perek & Kohoutek (1967). Early photographs of the nebulosity (Thackeray 1956; Westerlund & Henize 1967) suffer from contrast problems due to the apparent brightness of the central star AG Car. Stahl (1987) obtained direct CCD images of AG Car and its shell in several narrow-band filters. He derived a mass for the ionized gas which is consistent with the assumption that the nebulosity is due to ejection from AG Car itself.

Spectroscopic studies (Johnson 1976; Thackeray 1977) provided further evidence for a physical association of the nebulosities with AG Car. An expansion velocity of the shell of ~50 km s^{-1} with respect to AG Car was derived. This leads to a

[1] Based on observations made at the European Southern Observatory, La Silla, and at the Las Campanas Observatory.

[2] Space Telescope Science Institute, 3700 San Martin Drive, Baltimore, MD 21218.

[3] Affiliated to ESA, Astrophysics Division, Space Science Department of ESA.

[4] The Johns Hopkins University, Homewood Campus, Baltimore, MD 21218.

kinematic age of $\sim 10^4$ yr if a distance of 6 kpc is adopted (Humphreys et al. 1989). The nebular spectrum is characterized by many allowed and forbidden lines of low excitation. Strikingly, oxygen lines are weak or completely absent. In that respect the nebula around AG Car strongly resembles nebulosities around other luminous, evolved stars such as η Carinae (Davidson et al. 1986) or HD 148937 (Leitherer & Chavarría 1987; Dufour, Parker, & Henize 1988).

A spectacular result of high-resolution coronographic imaging (Nota & Paresce 1989; Paresce & Nota 1989) was the detection of bipolar and helical structures extending along the NE-SW directions of AG Car. The color of these structures suggests that the observed flux is primarily due to stellar light scattered by dust. Viotti et al. (1988) favored the same interpretation for the continuous energy distribution of the nebula observed in the *IUE* spectral region. A thermal equilibrium temperature of ~ 60 K has been derived for the dust from far-infrared measurements at 50 and 100 μm (McGregor et al. 1988).

More recently, a spectroscopic study of the nebular dynamics has been reported by Smith (1991). The study was performed with a spatial resolution of $\sim 2''$, spectral resolution of 7 km s^{-1}, at four slit locations, centered on the star. She finds evidence for a single shell expanding at 70 km s^{-1}, with the suggestion of bipolar outflow distorting the NE edge of the nebula that expands with a velocity of 83 km s^{-1}.

The unambiguous presence of axisymmetric structures in the nebulosities around AG Car may provide important clues for the ejection mechanism operating in luminous blue variables in general. In this paper we present a new, more detailed study of the nebular kinematics in an attempt to clarify the geometry of the system. Our study makes use of new high-resolution coronographic images, in the light of nebular emission lines and in broad-band continua, and of high-resolution, high signal-to-noise ratio long-slit spectroscopic data with complete coverage of the nebula.

2. OBSERVATIONS

New images of the AG Carinae nebula were obtained with the Adaptive Optics Coronograph (AOC) (Clampin, Golimowski, & Durrance 1991) at the Swope 40 inch telescope, Las Campanas. Since AG Carinae is bright ($V \simeq 8$ at the epoch of our observations), coronographic imaging is required if faint structures in the nebula are to be observed (see Paresce, Burrows, & Horne 1988 for a discussion). The AOC is unique in employing a tip/tilt mirror to compensate for image motion due to atmospheric turbulence and telescope jitter, resulting in improved angular resolution and enhanced contrast. Image motion is determined by reimaging the occulted central star onto a quadrant CCD which provides an offset to update the position of the tip/tilt mirror every 10 ms. The coronograph has an occulting mask followed by a lens which reimages the telescope exit pupil, where an apodizing mask suppresses diffracted light from the telescope optics. The lens provides a magnification of 5 at the coronograph focal plane where a Thomson 384 × 576 CCD detector yields a plate scale of $0''.13$ pixel^{-1} and a field of $50'' \times 74''$. On 1989 April 20, a Johnson V-band image was obtained in moderate seeing conditions of $1''.3$. The tip/tilt system improved the angular resolution to $\sim 1''.0$ and an occulting mask of $4''$ was used (Fig. 1). At that time, AG Carinae had a magnitude $V \simeq 7.9$. An additional Hα + [N II] image ($\lambda = 6560$ Å, $\Delta\lambda \simeq 110$ Å) was obtained on 1990 June 5 in similar seeing conditions with a modification to the coronograph yielding a plate of $0''.215$ pixel^{-1} (Fig. 2). At that time, AG Carinae had a magnitude $V \simeq 8$.

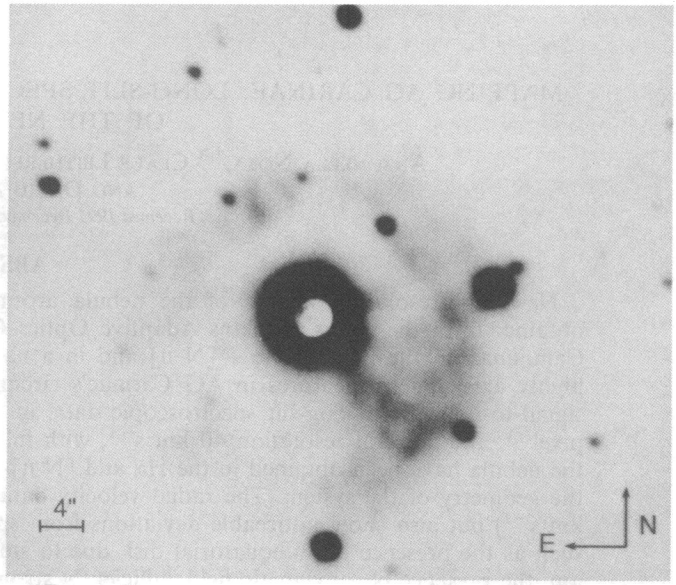

FIG. 1.—V-band image of AG Carinae obtained with the Johns Hopkins Adaptive Optics Coronograph, where north is at the top and east is to the left. The plate scale is $0''.13$ pixel^{-1} with a field of $50'' \times 74''$. The white spot at the center is the coronographic mask, $4''$ in size for this observation.

Spectroscopic observations of the AG Carinae nebula were made on 1990 February 18, at the ESO 2.2 m telescope, La Silla, with the Boller & Chivens Spectrograph coupled to a RCA CCD detector. The CCD, ESO No. 11, was selected for its good spectral response in the red, its relatively low dark current and its imaging format of 640 × 1024 pixels (15 μm in size), yielding a plate scale at the telescope of $0''.89$ pixel^{-1}.

The high-dispersion grating No. 22 (1200 grooves mm^{-1}, with a first-order dispersion of 59.5 Å mm^{-1}) was used, in conjunction with an order-blocking filter (OG-590) to prevent overlapping of unwanted orders in the spectral range of interest (6363–7254 Å). A projected slit width of $2''$ was chosen as a result of the prevalent seeing conditions $\simeq 1''.6$ FWHM.

A number of high signal-to-noise ratio He-Ar comparison spectra were obtained during the night to provide wavelength calibration of the spectra and to monitor the stability of the spectrograph. Dome flat fields were obtained at the beginning and at the end of the night, in order to calibrate the pixel-to-pixel nonuniformities, together with long dark exposures.

A total of 25 long-slit spectra were obtained at different locations on the AG Carinae nebula. The first step of the observational procedure was to acquire the star onto the slit, followed by a short exposure to verify the proper placement of the star, and, therefore, to fix a zero point for subsequent offsets, in addition to verify the instrumental setup. Spectral mapping was then started across the southern portion of the nebula. Increasing offsets of $-2''$ in declination were performed, until the visible region of the nebula, previously determined from our coronographic images, was fully mapped. The star was then reacquired and the nebula mapped toward the north, again using offset increments of $+2''$. An exposure time of 5 minutes was employed for each spectrum giving a signal-to-noise ratio for the Hα line varying between 500 in the brightest portion of the nebula and 250 at the very edges.

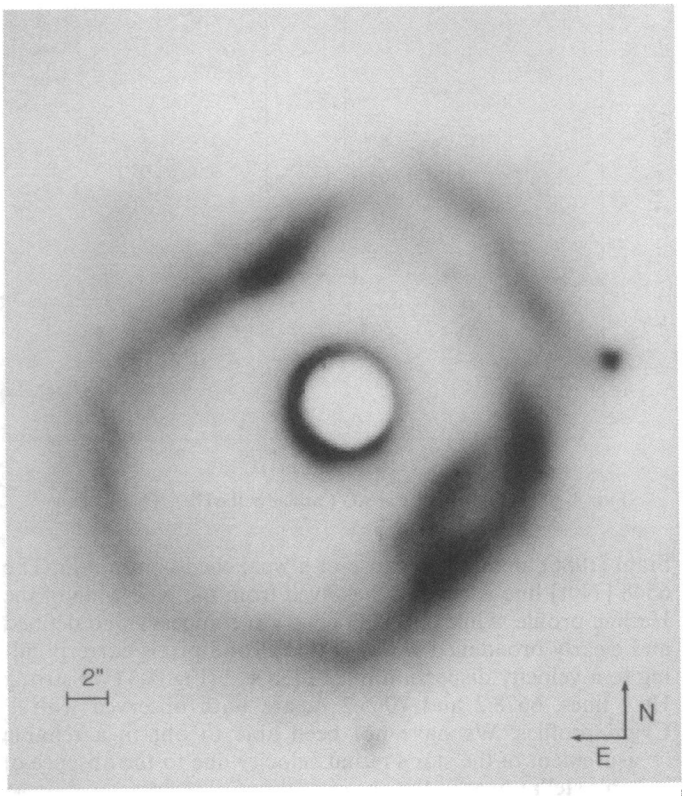

FIG. 2.—Hα + [N II] image of AG Carinae obtained with the Johns Hopkins Adaptive Optics Coronograph, where north is at the top and east is to the left. The plate scale is 0".22 pixel^{-1} with a field of 50" × 74". The white spot at the center is the coronographic mask, 5".8 in diameter.

Telescope pointing was continously checked for consistency by verifying the predicted location of the fainter stars that surround the AG Carinae nebula. From analysis of the spectra the overall accuracy in positioning the slit is estimated to be better than 1". The positions of the slits are shown in Figure 3, overlaid on a Hα band coronographic image of AG Carinae. In addition, spectra were taken of two spectrophotometric standard stars L745-46 and Kopff 27 (Oke 1974; Stone 1977), with the same instrumental configuration, to provide flux calibration of the science data.

3. DATA REDUCTION AND ANALYSIS

The basic reduction of spectroscopic and imaging data has been carried out according to the standard CCD data analysis procedures, i.e., all the frames have been bias- and dark-subtracted, divided by an average flat field and cleaned for cosmic rays. The spectra have been wavelength-calibrated using the He-Ar comparison spectra interleaved with the observations. The wavelength dispersion was calibrated by using the IRAF long-slit routine "identify" on the six comparison spectra obtained during the observations of AG Carinae. A fifth-order Chebyshev polynomial was fitted to 9–11 lines resulting in residuals of typically 0.1 pixel. The wavelength dispersion was determined to be 0.872 Å pixel^{-1} at Hα. All the spectra were flux-calibrated using the two spectrophotometric standard stars observed.

Following wavelength and flux calibration, the analysis of the spectra consisted of a detailed study of the emission lines at all spatial positions on the nebula, with the objective of constructing maps of the radial velocity variations, velocity dispersions, and line intensities to be then correlated with the optical images. A first inspection of the spectra showed clearly that the structure, as well as the central wavelength of the nebular lines varies with position around AG Carinae. There are areas where the lines are single, other areas in which a clear splitting is observed. The problem of determining radial velocities in both cases has been approached using the following procedure: first, we convolved the data in the direction of dispersion with a 1.91 pixel FWHM Gaussian, corresponding to the instrumental resolution, and determined the location of the line peaks by calculating the location and intensity value of peak of the parabola that is defined by the peak pixel and its two neighbors. The widths of the lines were estimated by calculating from the unconvolved data the location of the half intensity points, again using a parabola determined by the pixel closest to the half-intensity value and its two neighbors.

Then, a subset of spectra was selected for additional analysis based on the widths measured by the first method, that is, chosen using a region where the widths estimated from the first method exceeded 3.5 pixels. Areas with widths larger than 6.3 were also excluded since they were clearly associated with contamination from the bright star. This subset of data was analyzed by carrying out a two-component Gaussian fit where

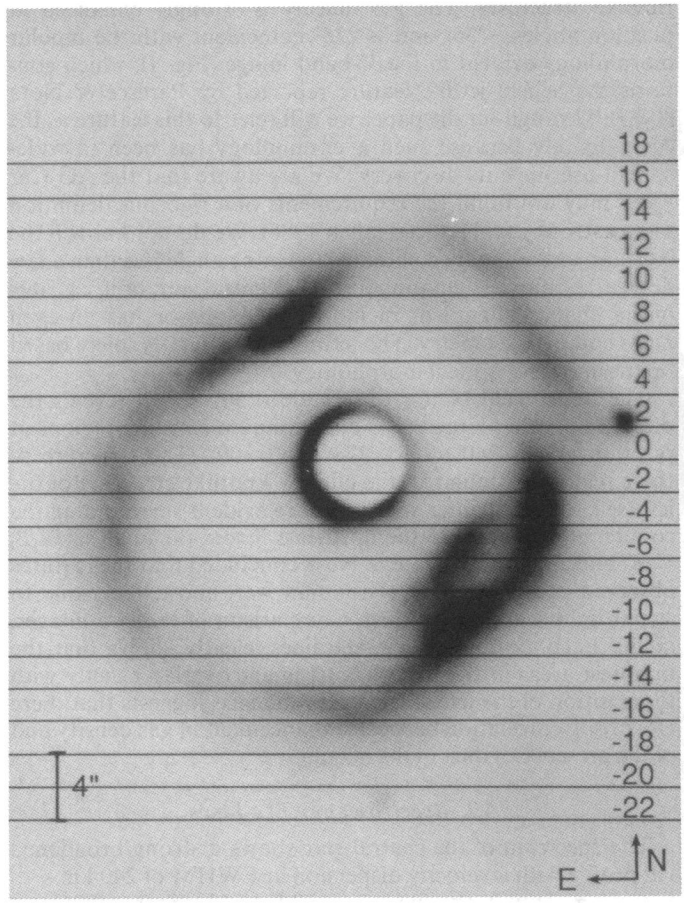

FIG. 3.—Hα + [N II] image of AG Carinae obtained with the Johns Hopkins Adaptive Optics Coronograph. The plate scale is 0".22 pixel^{-1} with a field of 50" × 74". The Hα + [N II] image is here displayed with the slit positions overlaid to illustrate our spectroscopic coverage of the nebula. The slit offsets are 2" with a slit width of 2".

the widths of the Gaussians were held fixed at 2.47 pixels and the amplitudes and locations of both Gaussians were allowed to vary. The fit was carried out using standard nonlinear least-squares fitting procedures with equal weighting of the data. All such fits were individually visually inspected for reasonableness. Most two component fits were good; a few were obviously poor—most of these bad fits were in the vicinity of the star—and were discarded.

The accuracy of the first method was checked by comparing the determined velocities of Hα lines between exposures that had been repeated at the same slit position (there were five such sets). These comparisons yield an rms error of 0.10 Å for all lines with peak intensities above 70 counts and well separated from the star (≃4″). This is primarily an estimate of the effect of noise on the fit and not of any systematic error or the effect of more complicated line structure than as assumed.

4. RESULTS

4.1. *Imaging*

The two coronographic images of the AG Carinae nebula display the general morphology previously observed by Stahl (1986) and Paresce & Nota (1989) but with an increased field of view covering the entire nebula. The Hα + [N II] (Fig. 2) image shows distinct deviations from spherical symmetry with the nebula appearing to be composed of two adjacent elongated ringlike structures. The gas density is strongly enhanced at position angles ∼35° and ∼225° coincident with the bipolar morphology evident in the *V*-band image (Fig. 1), which confirms the helical jetlike feature reported by Paresce & Nota (1989). Throughout the paper we will refer to this feature as the "jet," mainly because such a terminology has been in widespread use since its discovery. We are aware that the AG Car "jet" may not fulfill the requirements of a rigorous definition of an astrophysical jet (cf. Cohen 1986). We do not know if the AG Car jet is a highly collimated (opening angle less than a few degrees) outflow originating from the central star, or if, e.g., it is just a chance alignment of individual blobs or has an even more complex geometry. The terminology "jet" is solely based on the apparent optical morphology.

The larger field of this observation (50″ × 74″) reveals the presence of other large knots of continuum emitting regions at position angles 240°, 255°, 278°, and 300°. The structure of these regions is similar to the clumpy knotlike structure of the jet itself. Similar fainter structures are evident surrounding the counterjet extending to the northeast. From the analysis of *B*, *V*, *R*, and *I* colors, Paresce & Nota concluded that the features observed in the line-free continuum were most likely due to stellar light scattered by dust. Comparison of the two images, in the *V* continuum and in the lines, clearly shows that the brightest areas in the Hα + [N II] image overlap exactly with the position of the jet. This correspondence suggests that there is a strong correlation between enhancement of gas density and of the presence of dust in the nebula.

4.2. *Spectroscopy: The Lines*

The spectrum of the central star shows a strong broadened Hα profile with a velocity dispersion at FWHM of 240 km s^{-1}. In agreement with the spectrum published by Stahl (1986), we do not observe evidence for a P Cygni profile previously detected by Viotti et al. (1984) in the 1980/1981 phase. We observe both [N II] emission lines at 6548 and 6583 Å, which appear to have grown stronger since the spectra published by Stahl (1986), possibly because of a weakened continuum. The 6548 [N II] line is not fully resolved from the blue wing of the Hα line profile, while the 6583 [N II] line appears well defined and clearly broadened with a FWHM of 8 pixels corresponding to a velocity dispersion of 320 km s^{-1} (Fig. 4). Two strong He I lines, 6678.2 and 7065.2 Å, are both observed with P Cygni profiles. We have not been able to obtain a reliable measurement of the star's radial velocity due to the absence of suitable stellar lines in the observed spectral region.

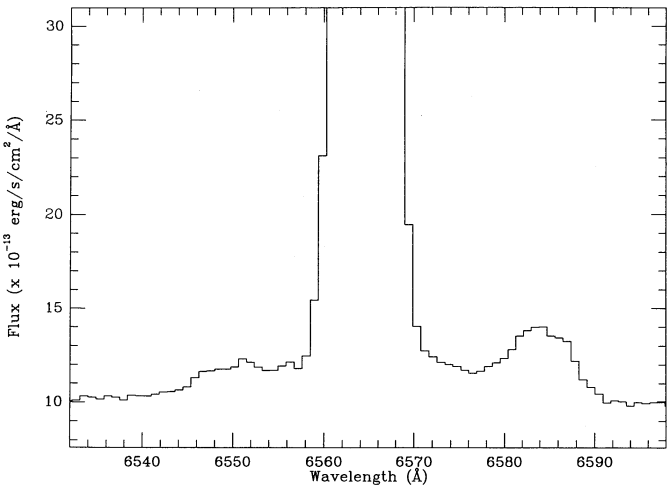

FIG. 4.—Spectrum of the star AG Carinae in the Hα + [N II] region

In all the spectra taken on the nebula, five nebular emission lines are clearly detected at various strengths and widths according to the position of the slit with respect to the central star: Hα (6563 Å), [N II] (6548 Å), [N II] (6583 Å), [S II] (6716 Å), and [S II] (6731 Å).

For the purpose of mapping the dynamics of the gas in the nebula, radial velocities have been determined in three of these lines, namely Hα and the two [N II] lines. The measurements derived from the line-fitting procedure described in the previous section have been converted to radial velocities and corrected to the local standard of rest (LSR). The overall resolution of our data is 40 km s^{-1}, and no attempt has been made to subtract the systemic radial velocity. Figure 5 shows the radial velocity curves for Hα obtained at six different slit locations on the nebula. In all cases the slit is oriented E-W. In this figure the abscissa scans the positions along the slit in arcseconds from east to west where position zero represents the location of the star, while the ordinate is the LSR radial velocity in km s^{-1}. Comparison of the Hα maps and the [N II] 6583 Å maps present perfect overlap, in the single- and double-component region. Good agreement is shown also by the [N II] 6548 Å, even though the weaker line results in a noisier set of maps that will not be included in this discussion. The six selected positions, spanning 12″ south to 12″ north give an overall representation of the dynamical structure of the nebula: the clear line splitting observed, more pronounced in a region extending 15″ southeast from the star, is consistent with a hollow shell of expanding gas, in agreement with Thackeray (1977) and Smith (1991). A comparison with the coronographic images shows that this area has a low surface brightness and, therefore, low gas density. In the region where line splitting occurs, we can resolve at most two individual line components even though in some cases the line profiles are suggestive of multiple components. As a result, some radial velocity mea-

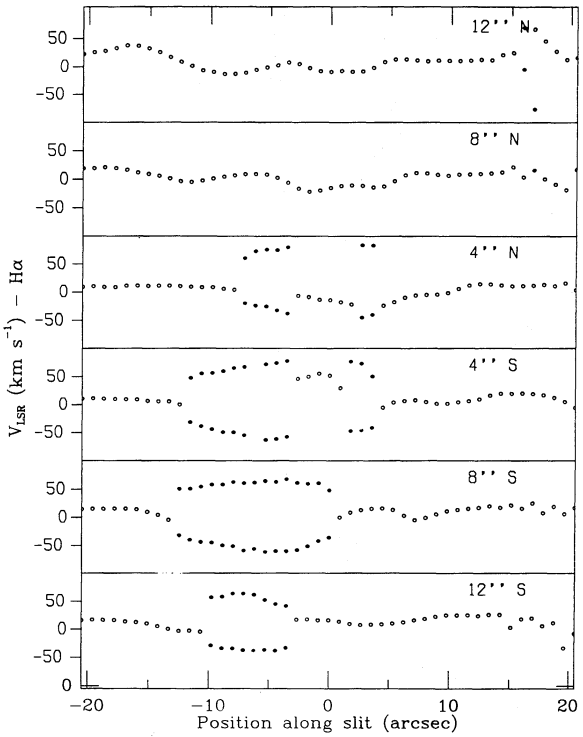

FIG. 5.—Radial velocity curves for six selected slit positions in the Hα line. In all cases the slit is oriented E-W. The abscissa scans the positions along the slit in arcseconds from east to west where position zero represents the location of the star, while the ordinate is the LSR radial velocity in km s^{-1}. The white dots represent regions where only a single component was detected; the filled dots indicate line splitting and detection of two components.

surements have been deleted in cases where the line-fitting procedure was unable to find a satisfactory solution.

From the line splitting observed close to the star, we derive an average expansion velocity for the shell of 70 km s^{-1}, in agreement with Smith (1991). In addition, we observe local variations from the average radial velocity, mainly concentrated along the axis defined by the jet and counterjet. These variations are more pronounced toward the southwest and are clearly apparent in the 8″ S subset of Figure 5, at 7″ W from the star, with an amplitude of 10–20 km s^{-1}. This position corresponds, in the *V* image (Fig. 1), to the brightest region of the jet. An expanded view of all the radial velocity profiles in the southwest quadrant tracks the evolution of the variations with position. This is shown in Figure 6 where, for display purposes only, we have subtracted from the LSR radial velocities the currently accepted value for the systemic velocity of 7 km s^{-1} (Stahl 1986; Smith 1991). Similar behavior is observed in the radial velocity structure in the northeast quadrant, although at a slightly lower amplitude level (10–15 km s^{-1}). These values are significant considering that the overall accuracy of our determinations is better than 4 km s^{-1}.

An alternative method for the display of the radial velocity data is presented in Figure 7, where we show a composition velocity of two images: the first, in gray scale, has been generated by assigning to each spatial position its corresponding radial velocity value. The gray-scale image is superposed on a second intensity contour plot of the nebula in Hα + [N II] (corresponding to Fig. 2). The gray scale is displayed with intensity values set between −20 km s^{-1} (black) and +20 km s^{-1} (white), respectively, in order to enhance small-amplitude radial velocity variations. The central white spot is the bright star, and the adjacent (black) region corresponds to the areas in the nebula where two line components were resolved and measured. These values have been excluded in the generation of the radial velocity map. The local radial velocity variations shown in Figure 6 are clearly seen in this image as several discrete regions running perpendicular to and distributed along the NE-SW axis, which appear to be associated with the structures observed in the images of the nebula. There is definite evidence for a deviation from spherical symmetry in the radial velocity structure, as we already noted for the gas distribution observed in the coronographic images (Figs. 1 and 2).

4.3. *Spectroscopy: the Continuum*

Paresce & Nota (1989) found the color of the jet to be suggestive of scattering of stellar light by dust distributed in different areas of the nebula. This conclusion is in agreement with the IR observations of McGregor et al. (1988) and ultraviolet observations of Viotti et al. (1988).

Part of the continuum can also be explained in terms of thermal free-free and free-bound radiation from hydrogen and helium, as well as of the two-photon decay of the 2 ^2S level of H I. We estimated the expected strength of the *nebular continuum* from the observed emission-line fluxes. The total recombination coefficient for the continuum can be written as

$$\gamma_\nu(\mathrm{tot}) = \gamma_\nu(\mathrm{H}^0) + \gamma_\nu(\mathrm{He}^0) + \gamma_\nu(2q)\ . \qquad (1)$$

The individual coefficients account for free-free and free-bound continua of hydrogen and helium and for the two-photon decay in H I. It is assumed that He has normal abundance and

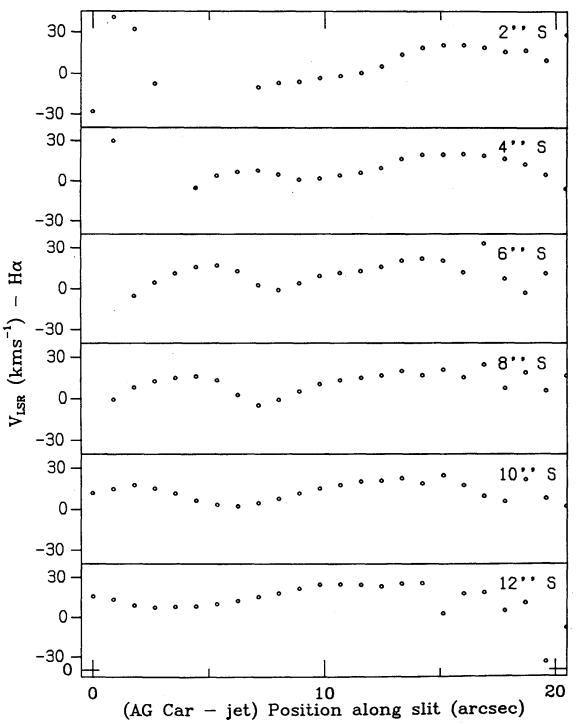

FIG. 6.—Variation of radial velocity in the southwestern region of the nebula, corresponding to the location of the jet feature. The abscissa scans the positions along the slit in arcseconds from the location of the star to 20″ west, while the ordinate is the LSR radial velocity in km s^{-1}. Only the data in which a single component was detected are shown here.

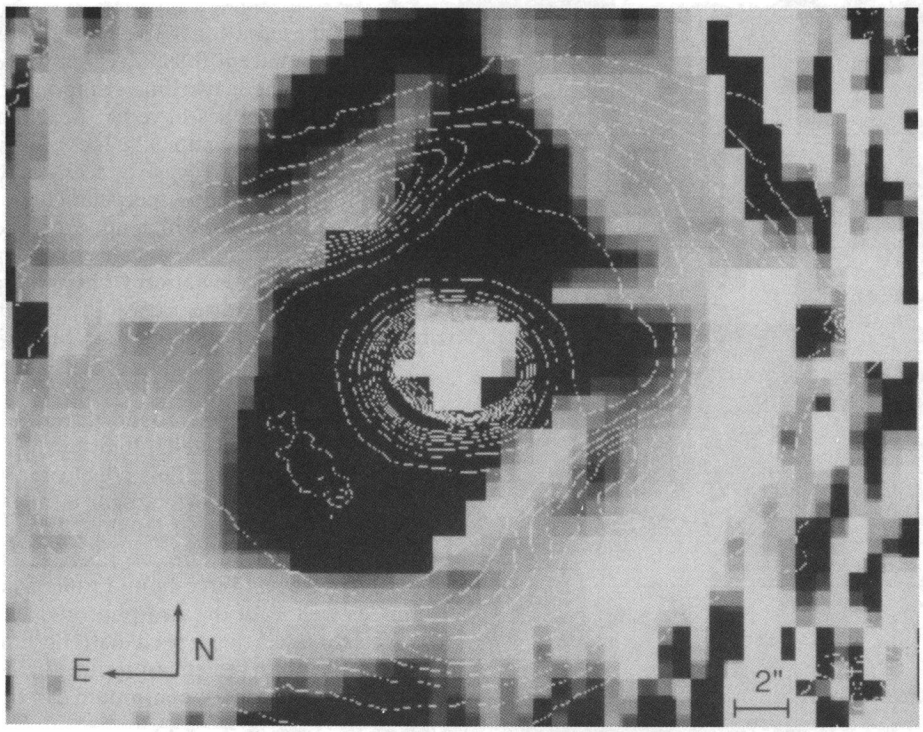

FIG. 7.—Bidimensional radial velocity map represented as a gray-scale overlaid on the contour plot of the Hα coronographic image shown in Fig. 2. The gray scale is displayed with intensity values set between -20 km s^{-1} (black) and $+20$ km s^{-1} (white), respectively, in order to enhance small-amplitude radial velocity variations. The central white spot is the bright star, and the adjacent (black) region corresponds to the areas in the nebula where two line components were resolved and measured. These values have been excluded in the generation of the radial velocity map.

that He II can be neglected. The former assumption possibly is a slight underestimate of the actual He abundance but is of minor consequence in the present context. Using Osterbrock's (1989) tabulation we estimate that $\gamma_\nu(\mathrm{He}^0) \approx 9 \times 10^{-40}$ ergs cm^{-3} s^{-1} Hz^{-1}, $\gamma_\nu(\mathrm{H}^0) \approx 7 \times 10^{-40}$ ergs cm^{-3} s^{-1} Hz^{-1}, and $\gamma_\nu(2q) \approx 2 \times 10^{-40}$ ergs cm^{-3} s^{-1} Hz^{-1} for $T_e = 10{,}000$ K and $\lambda = 6563$ Å so that $\gamma_\nu(\mathrm{tot}) \approx 1.4 \times 10^{-28}$ ergs cm^{-3} s^{-1} Å^{-1}. The Hα recombination coefficient is $\gamma(\mathrm{H}\alpha) = 3.5 \times 10^{-25}$ ergs cm^{-3} s^{-1}. Therefore continuous emission contributes approximately 4% to the total flux measured in a filter of bandwidth 110 Å centered on Hα. We can use this estimate to predict the nebular emission within the *V* filter. The flux observed with the Hα filter in the brightest part of the SE jet is 1.1×10^{-13} ergs cm^{-2} s^{-1} arcsec^{-2}. Neglecting any wavelength dependence of the nebular continuous emission (both due to atomic physics and extinction), we expect a flux of approximately 2.9×10^{-14} ergs cm^{-2} s^{-1} arcsec^{-2} at the wavelength of the *V* filter. The value may actually be a conservative upper limit as we neglected any flux contribution from the [N II] lines when we derived the continuous emission in the Hα filter. The surface brightness of the same portion of the jet measured on our *V* image ($\Delta\lambda = 740$ Å) is 17.9 m arcsec^{-2}, or 1.9×10^{-13} ergs cm^{-2} s^{-1} arcsec^{-2}. This value is much higher than expected on the basis of nebular continuous emission. Consequently the observed continuum is predominantly due to reflected stellar light from AG Car with a small (<15%) additional contribution from nebular continuum emission. Moreover, we detect in the nebular spectra reflected, bright stellar emission lines, appearing as underlying broadened components superposed on the nebular lines. This emission-line structure is most prominent in the Hα line profiles, as is shown in Figure 8, where an Hα line profile shows the the weak high-velocity wings which are absent in the two [N II] lines. The width of these wings is estimated to be ~300 km s^{-1} and agrees, within the errors of our measurements, with the width of Hα in AG Car itself suggesting that stellar light is scattered by dust particles in the nebula. The stellar Hα is Doppler-broadened by a stellar wind flowing at ≃240 km s^{-1}. The same Doppler broadening is present in the stellar [N II]. However, the relative weakness of the *stellar* [N II] emission with respect to Hα

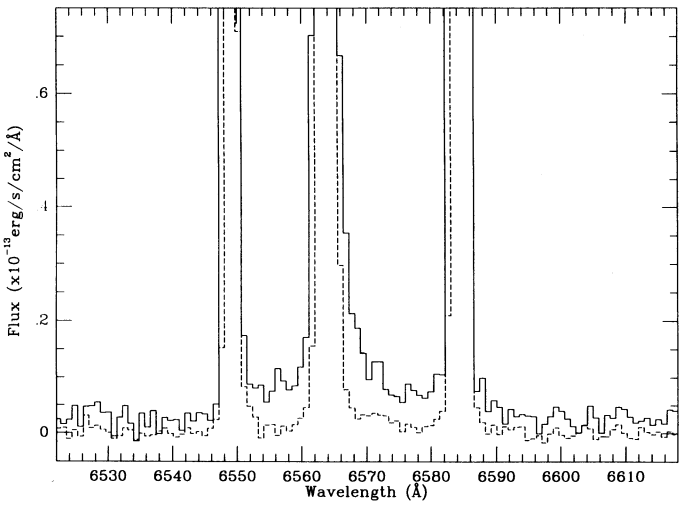

FIG. 8.—Broadened, reflected stellar Hα line superposed on the narrow nebular Hα emission line. The two spectra shown are extracted from the 8″ S slit position. The spectrum that shows the broadened reflected stellar line is extracted at the location of the brightest knot of the jet (W); the second spectrum is extracted in the E, at the same angular distance from the star.

precludes the detection of high-velocity wings due to stellar [N II] in the nebular [N II] lines.

Both effects, reflected stellar continuum and presence of broadened emission lines, are highly position dependent. The stellar continuum, for example, is well detected in the southwest and northeast quadrants and, to a lesser extent in the northwest quadrant. It is almost undetectable toward the southeast. In order to visualize our findings, we have generated a continuum map (Fig. 9) from our long-slit data. For each slit position, we have fitted the continuum over the spectral range 6363–6886 Å, excluding the nebular emission lines. The fitted spectra have then been integrated in the dispersion direction to produce a one-dimensional profile of the integrated continuum along the slit. All the continuum profiles have then been stacked to reconstruct a two-dimensional map of the nebula. The locations of the field stars and AG Carinae itself are marked on the map, to facilitate comparison with the V band image (Fig. 1). In the interval between slit positions 2″N to 2″S the contamination, due to scattered light from AG Carinae, dominates. In the southwest quadrant, in addition to detecting three field stars we also see diffuse emission resembling the structure and orientation of the jet feature. Similarly in the NE, although there is contamination from unresolved field stars.

5. DISCUSSION

The velocity field derived from our long-slit spectroscopy strongly suggests a physical connection between the gaseous material and AG Carinae itself. Such a conclusion has also been reached by Smith (1991). We note that the distance of AG Car is relatively uncertain since it is not a member of a known cluster or association. Humphreys et al. (1989) presented evidence that AG Car does not belong to either Car OB1 or Car OB2 and suggested a distance of 6 kpc. Their conclusion is based on a study of the extinction of surrounding field stars and on the kinematics of the Carina spiral arm. Assuming a distance of 6 kpc to AG Car, the dynamical time scale for the outer ringlike structure turns out to be $\sim 10^4$ yr. Revisions of the distance to AG Car would affect this value. In addition, significant acceleration or deceleration zones may also modify the time scale. In any case, we may conclude that an age of $\sim 10^4$ yr is consistent with the assumption that the nebulosities originated in an explosive event in AG Car itself.

The nebulosities show distinct deviations from spherical symmetry: in the spectra, the line splitting observed in Hα and [N II] appears most pronounced along the northwest-southeast direction. From the images, the elliptical nebula appears to have a two-layered structure, and it is evident that the gas density is strongly enhanced at position angles $\sim 35°$ and $\sim 225°$, coincident with the outermost regions of the northeast and southwest jets, respectively. This suggests a physical connection of the jets and the outer layer. Figure 10 shows the ratio of the [S II] lines $I(6716)/I(6731)$ for a slit position in the east-west direction 6″ north of AG Car. The [S II] line ratio suggests a maximum electron density of $\sim 10^4$ cm^{-3} in the visually brightest parts of the nebula. However, close inspection of Figure 10 demonstrates a highly nonuni-

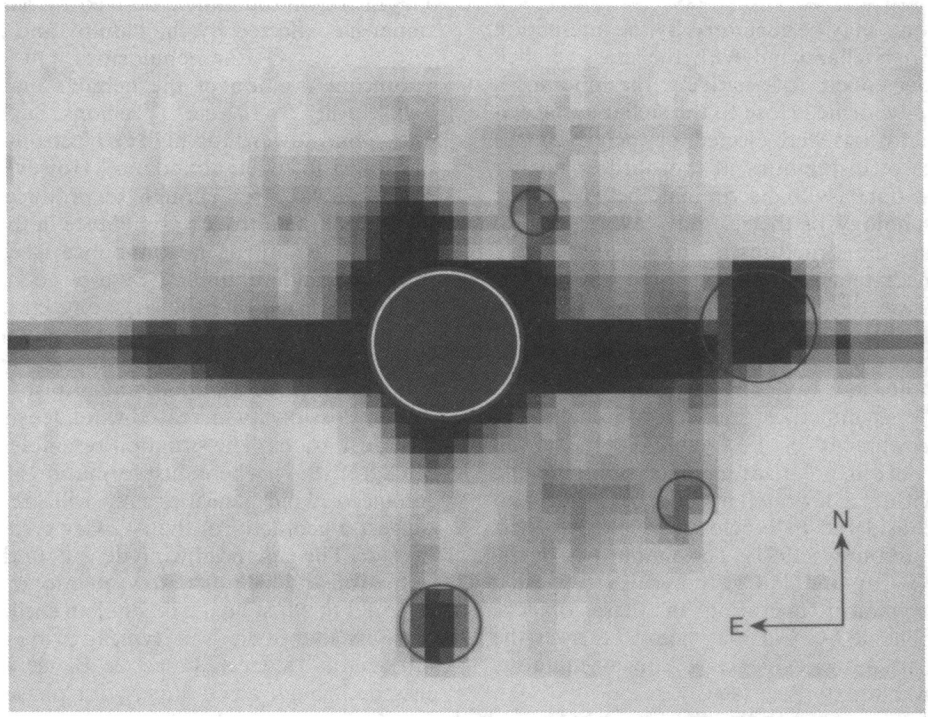

FIG. 9.—Map showing the integrated continuum in the spectral range, excluding the nebular emission lines. The locations of the field stars and AG Carinae itself are marked on the map, to facilitate comparison with the V-band image (Fig. 1). In the interval between slit positions 2″N to 2″S the contamination, due to scattered light from AG Carinae, dominates. In the SW quadrant, in addition to detecting three field stars, we also see diffuse emission resembling the structure and orientation of the jet feature. Similarly in the NE, although there is contamination from unresolved field stars.

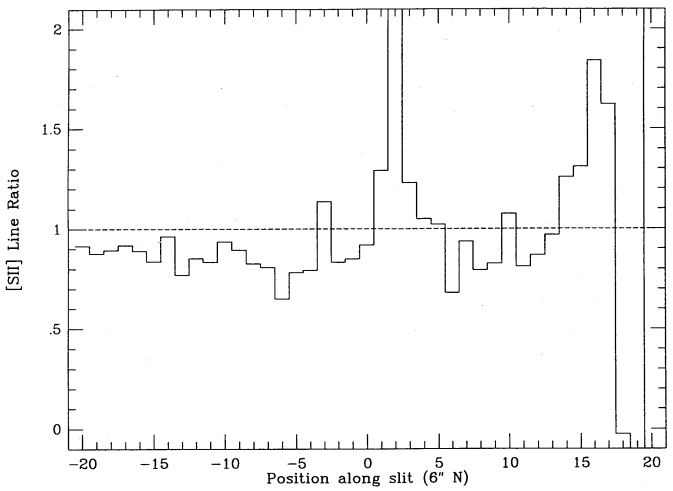

FIG. 10.—The ratio of the [S II] lines $I(6716)/I(6731)$ for a slit position in the east-west direction, 6″ north of AG Car. In abscissa east is on the left and the position with respect to the star is indicated in arcseconds.

form density distribution even in these brightest nebular regions. The line ratio $I(6716)/I(6731)$ indicates density variations by a factor of ~ 10 over a scale 2″–3″. This is in accord with the rather inhomogeneous structure of the entire gas and dust around AG Car (Fig. 2). The structure of the nebula is made of filaments and blobs. Hester et al. (1991) discussed the morphology of the nebulosities surrounding the LBV η Carinae, resolved by *Hubble Space Telescope* into a series of knots with a scale of about 0.″3. The similarities of the nebulosities surrounding AG Car and η Car may hint at related mechanisms responsible for the formation of these structures in both objects.

The knots and filaments may be generated by the interaction of AG Car's continuous stellar wind with the massive shell ejected during an earlier epoch. Alternatively, the inhomogeneities could have already formed close to the stellar surface at the time when the nebulosities were ejected, or their existence may be a consequence of instabilities in the outflow farther away from the star. It is not easy to discriminate between these possibilities. The morphology of the jet may favor a site of origin close to the star: the structures in the jet are already discernible in the immediate surroundings of the central star (as close as 5″). In this case, the ejection mechanism would be a highly time-dependent, stochastic phenomenon rather than a smooth, stationary process.

It is interesting to note that Taylor et al. (1991) also found evidence for large-scale asymmetries and inhomogeneities in the circumstellar environment of P Cygni. Taylor et al. deduced this geometry from polarization data sampling the stellar environment within a few stellar radii. AG Car and P Cyg are generally considered to be closely related in their evolutionary status (Humphreys 1991). The similarities in the wind properties of AG Car and P Cyg may also suggest a common ejection mechanism operating in these objects. Polarimetric observations of AG Car may help to answer the question if AG Car also shows evidence for an asymmetric, inhomogeneous outflow close to its surface.

The large density variations across the AG Car nebulosities make any mass estimate rather difficult. If we assume an average electron density of 500 cm^{-3} for the ring at a minimum and maximum radial distance of 10″ and 14″, respectively, an ionized gas mass of $\sim 3.5\ M_\odot$ is derived. The uncertainty is large, though. Depending on the adopted nebular geometry and mass distribution, this estimate could be off by a large factor.

As an alternative, the ionized mass of the nebula can be derived from the integrated, extinction-free emission-line luminosity and the electron density. The integrated Hα flux obtained from the coronographic images is 3.8×10^{-11} ergs $cm^{-2}\ s^{-1}$. This value has been derived by measuring the integrated flux in the Hα image, after subtraction of the background and of the central star. The Hα image had previously been flux-calibrated with observations of photometric standard stars observed during the same night. The extinction-corrected values then follow from Whitford's (1958) extinction law together with $E(B-V) = 0.63$ (Humphreys et al. 1989): $F_{H\alpha} = 1.6 \times 10^{-10}$ ergs $cm^{-2}\ s^{-1}$. Using the relation $M = 3.87 \times F_{H\alpha} D^2 T_e^{0.85} n_e^{-1}$ (Pottasch 1980), the ionized gas mass can be derived from the emission-line flux $F_{H\alpha}$, distance D, electron temperature T_e, and electron density n_e. The mass thus obtained is $4.2\ M_\odot$. $T_e = 9000$ K (Mitra & Dufour 1990) and $n_e = 500$ cm^{-3} have been assumed in deriving the nebular mass. The reasonable agreement between the masses derived via both methods gives some confidence in our mass estimate.

Mitra & Dufour (1990) studied the chemical composition of the AG Car ring nebula. They found a very high value of log (N/O) of ~ 0.3. Such a number is also typical for the condensations around η Carinae (Davidson et al. 1986) or for the bipolar ejecta around HD 148937 (Dufour et al. 1988). However, in contrast to η Car or HD 148937, the AG Car nebula has only a very moderate—if any—overabundance of nitrogen. The large N/O ratio is predominantly due to an extremely low oxygen abundance. Already Caputo & Viotti (1970) had noticed an oxygen anomaly in the AG Car nebula. The nitrogen abundance derived by Mitra & Dufour may be somewhat affected by the clumpy and inhomogeneous structure of the AG Car nebulosities. Our results suggest that a significant fraction of the nebular material occurs in small, high-density ($\sim 10^4$ cm^{-3}) regions. Such structure may introduce a bias toward too high an electron temperature and hence too low a nitrogen abundance. However, it is not clear if this effect can be large enough to produce a significant upward revision of the nitrogen abundance in the AG Car nebulosities. Possibly, the nitrogen abundance is close to solar, whereas oxygen is underabundant by a large factor. Mitra & Dufour (1990) suggested that the large oxygen underabundance is due to oxygen (and possibly carbon) being locked into dust. Most of the observed dust is in the bipolar jet and also in the ring nebula. It is not clear what makes dust formation so efficient in the jet. Possibly an increased wind density helps to lock oxygen into dust grains. The situation resembles the case of B[e] stars (Zickgraf 1989), where dust formation also occurs in regions of enhanced wind densities. As will be discussed below, we suggest a geometry of the AG Car system with a disk around the star. The enhanced wind density in the disk may favor dust formation and locking of oxygen into grains.

Could the dust be the relict of an earlier evolutionary phase? Circumstellar dust is a typical property of many late-type supergiants (Stencel, Pesce, & Bauer 1988). If AG Car had passed through a red supergiant phase earlier in its history, dust formation might have occurred at that time. There are two possible problems with this interpretation. First, the evolutionary time scale for a massive star to become a blue supergiant after the red supergiant phase is larger than 10^4 yr

(Langer & El Eid 1986; Maeder 1990), i.e., larger than the age of the ejecta based on the dynamical time scale. Second, the currently favored distance—and thus luminosity—does not support the hypothesis that AG Car ever passed through the red supergiant phase. Evolutionary models (e.g., Maeder 1990) exclude a red supergiant phase for stars above $M > 50\,M_\odot$.

The radius of the Strömgren sphere resulting from AG Car's ionizing radiation can be estimated via Osterbrock's (1989) tabulation. We assigned an equivalent spectral type of O9 I to AG Car in its hottest phase. Spectral type O is indicated by the presence of broad He II λ4686, visible in spectra taken close to the time of our observations (V. F. Polcaro, private communication). With $\log L = 10^{6.2}\ L_\odot$ (Humphreys et al. 1989) and $T_{\rm eff} = 30{,}000$ K, a radius of $R = 46\ R_\odot$ is found. Using Leitherer's (1990) spectral type versus $N_{\rm L}$ calibration, the total output of ionizing quanta in the Lyman continuum is $N_{\rm L} = 10^{49.83}\ {\rm s}^{-1}$. Therefore we have $N_e N_p r_1^3 = 10^{6.23}$ in Osterbrock's notation, where r_1 is the radius of the Strömgren sphere in pc. Adopting $N_e = N_p = 500\ {\rm cm}^{-3}$, we find that the shell of inner and outer radius of 0.3 pc and 0.4 pc (corresponding to angular radii of 10″ and 14″, respectively) can easily be ionized. This result suggests that the AG Car nebula is density-bounded. We note that the recombination time scale ($\approx 1/(\alpha_B n_e)$, where α_B is the case B recombination coefficient for hydrogen) is long ($\sim$250 yr) in comparison with the typical time scale associated with the recurrence of LBV variations ($\sim$10 yr). Therefore, the nebula will remain ionized even when the star enters a phase of lower temperatures.

It is generally predicted that LBVs show signatures of CNO processing on their surface. Evolutionary models (e.g., Maeder 1990) predict a significant enrichment of nitrogen and depletion of oxygen and carbon on the stellar surface in the course of the LBV phase. In fact, abundances derived for the η Car nebulosities agree with theoretical models predicting CNO equilibrium in later stages of the LBV phase (Maeder 1989). On the other hand, the nitrogen abundance derived for the AG Car nebula by Mitra & Dufour (1990) suggests no significant nitrogen enrichment. We interpret the different nitrogen abundances in the nebulosities around AG Car and η Car as a result of their different dynamical time scales relative to the LBV lifetime.

The lifetime of the LBV phase is difficult to estimate observationally due to small number statistics. It is generally assumed to be about 10^4 yr or somewhat higher (Humphreys 1991). Interestingly, this is the same order of magnitude as the dynamical time scale of the ring nebula around AG Car. In contrast, the dynamical time scale for the knots observed around η Car is much shorter. Walborn, Blanco, & Thackeray (1978) measured proper motions for discrete features in the outer shell of η Car on plates taken at two different epochs. From the deduced tangential velocities these authors derive a dynamical time scale of 10^2–10^3 yr. A subsequent study by Walborn & Blanco (1988) using third-epoch proper motion measurements suggests that the slowest material around η Car underwent significant deceleration. Therefore, most or even all of the material may have been ejected about 150 years ago during the great light maximum of the 1830s and 1840s. In contrast, the nebulosities around AG Car were ejected 10^4 yr ago when AG Car was just at the beginning or in the earliest phases of the LBV stage when the CNO equilibrium was not yet reached. Therefore, the different dynamical time scales of the AG Car and η Car nebulosities may explain the different abundance patterns found. No detailed *photospheric* abundance analysis of AG Car has yet been done. Walborn (1989) discussed the photospheric spectrum of AG Car and concluded from the optical morphology that it is virtually certain that a large nitrogen overabundance will be found. This suggests that AG Car has now entered the CNO equilibrium phase as evident from the present-day photospheric spectrum. On the other hand, if the nebular analysis is correct, the abundances reflect a state $\sim 10^4$ yr ago when AG Car still had helium and heavy element abundances typical for massive blue supergiants.

6. CONCLUSIONS

The optical morphology of the nebula around AG Car suggests a basically bipolar structure. Such a structure is evident from our broad-band V images, which show reflected stellar light in the bipolar jet and from our narrow-band Hα images where the regions of enhanced gas density are aligned with the two optical jets. Understanding the mechanism responsible for the ejection of gas and dust from the central star is a prerequisite for an interpretation of the jet and shell geometries. Traditionally, LBV eruptions are assumed to be related to atmospheric (e.g., Lamers & Fitzpatrick 1988) or structural (e.g., Maeder 1989) instabilities occurring in massive, single stars. Although the importance of stellar rotation has been emphasized (Sreenivasan & Wilson 1989), all *quantitative* models essentially assume a spherically symmetric geometry for the stellar system and deviations from such symmetry are not taken into account. The observational data of AG Car clearly are at variance with such models.

What could break a spherically symmetric geometry in AG Car, leading to an essentially axisymmetric configuration of the outflow? The most plausible scenarios appear to be a magnetic field and/or an equatorial disk in AG Car. It is interesting to note that an equatorial disk model has also been proposed for B[e] stars (Zickgraf et al. 1986). B[e] stars are located in about the same region of the HRD, yet their evolutionary relation to LBVs is unclear (see Zickgraf 1992 for a review). However, we may conclude that there are at least some stars in this part of the HRD where the outflow characteristics are controlled by circumstellar disks. The origin of these disks is an open issue. Stellar rotation or a close binary companion may play a role. A density enhancement in the equatorial plane may be produced by stellar rotation close to the break-up velocity, leading to a slow equatorial outflow and a focusing effect for the wind along the polar axis.

As an alternative, the presence of a disk may be due to a close companion star. Kenyon & Gallagher (1985) presented a binary model for LBVs where the eruption is a consequence of strong mass accretion from a Roche lobe–filling primary by a secondary star. The accretion-powered binary model was subsequently criticized due to the excessively high accretion rates required to account for the observations (Gallagher 1989). In addition, the restriction of the LBV phenomenon to a relatively small part of the HRD is difficult to understand in such a binary scenario.

About one-third of all O stars occur in binary systems (Garmany, Conti, & Massey 1980). Since LBVs are considered the evolved counterparts of the most massive O stars (Humphreys 1989; Maeder 1989), one would expect a sizable fraction of LBVs to occur in binary systems, too. The only established binary among the LBVs is the LMC object R81, which was shown to be an eclipsing binary by Stahl, Wolf, & Zickgraf (1987). Could AG Car also be a binary system com-

posed of a primary and a yet undetected companion? The mechanism triggering the LBV phenomenon may entirely be due to the primary. The secondary merely accretes part of the material lost from the primary by an accretion disk and gives rise to the bipolar jet perpendicular to the disk. The nature of the secondary is unknown. There is no indication for the presence of a companion from photometric or radial velocity studies of AG Car (see Caputo & Viotti 1970). Also, the continuous energy distribution of AG Car agrees with the emergent flux expected for a single early-type star (Humphreys et al. 1989). Since the equivalent spectral type of AG Car varies from late O to early A, at certain times a cooler or hotter companion would be detectable in the red or ultraviolet spectral region, respectively. Alternatively, one can hypothesize the presence of an unseen, compact companion, such as a neutron star. The neutron star is surrounded by an accretion disk and is responsible for the bipolar jet in the AG Car system. One should be aware that there is no direct observational evidence for such a scenario. In that respect AG Car resembles the WN5 star HD 50896 where the presence of an unseen, compact companion has also been suggested (Drissen et al. 1989).

An interpretation of AG Car as a binary system helps to interpret the bipolar structure of the ejecta surrounding the system on the one hand, and it avoids the problems inherent in Kenyon & Gallagher's (1985) original model on the other. In the present scenario, the mechanism responsible for the LBV phenomenon is entirely due to the primary—strong mass loss in certain evolutionary phases would occur even without the companion. A secondary star is expected in *some* LBVs on statistical reasons and can strongly influence the geometry of the material ejected by the system.

If a magnetic field of sufficient strength were present in AG Car, the presence of the bipolar outflow could possibly be understood without invoking a binary model. Aitken et al. (1990) proposed a hydromagnetically driven wind for MWC 349, a related object. MWC 349 is a hot, luminous emission-line star surrounded by a bipolar nebula. Like AG Car, MWC 349 is surrounded by circumstellar dust which is not the relict of an earlier evolutionary phase but is currently being formed in the wind (White & Becker 1985).

It is conceivable that the observed structures are purely a consequence of the physical conditions of the surrounding interstellar medium. Königl (1982) and Raga & Cantó (1989) studied the effect of anisotropic density and pressure distributions of the interstellar medium on a spherically symmetric stellar wind. The density gradient creates an elongated bubble which subsequently becomes unstable to the formation of de Laval nozzles. The de Laval nozzles can channel the flow into supersonic jets. This model has originally been applied to bipolar outflows from young stellar objects, like Herbig-Haro objects. However, the physical conditions of AG Car and its surrounding interstellar medium may be similar to the situation in young stellar objects, and the asymmetric structures observed around AG Car may be the signatures of pressure and density gradients in the environment.

Presently we cannot decide which—if any—of the proposed models for AG Car is correct. The clue for understanding the AG Car nebula and jet may lie in the central star itself. What is the relation between the stellar wind (within $\sim 10\ R_{\rm phot}$) and the gas at a distance of ~ 1 pc from the star? Observational studies (e.g., using spectropolarimetry) of the wind geometry will be crucial for our interpretation of AG Car, and of LBVs in general. Impressive progress in detecting asymmetric outflows in Wolf-Rayet stars by spectropolarimetric techniques has recently been made (Schulte-Ladbeck, Meade, & Hillier 1992). Extension of such studies to LBV winds is currently underway by our group. Ultimately, we hope to recognize and understand the importance of asymmetric outflows for the physics of LBVs. Possibly, AG Car is not an exotic exception in the life of a massive star but is a rather normal case of a star undergoing heavy mass loss.

The authors are grateful to Francesco Paresce and Nino Panagia for many useful discussions and suggestions. The development of the Johns Hopkins Adaptive Optics Coronograph has been supported from the Seaver Institute and the Center for Astrophysical Sciences. M. C. and D. A. G. thank the Carnegie Institution for the award of telescope time at the Las Campanas Observatory.

REFERENCES

Aitken, D. K. Smith, C. H., Roche, P. F., & Wright, C. M. 1990, MNRAS, 247, 466
Bond, H. E., & Landolt, A. U. 1970, PASP, 82, 313
Cannon, A. J. 1916, Harvard Ann., 76, No. 3
Caputo, F., & Viotti, R. 1970, A&A, 7, 266
Clampin, M., Golimowski, D., & Durrance, S. 1991, in Active and Adaptive Optical Systems, ed. M. Ealey (Proc. SPIE, 1542), 165
Cohen, M. 1986, in IAU Symp. 116, Circumstellar Matter, ed. I. Appenzeller & C. Jordan (Dordrecht: Reidel), 39
Davidson, K., Dufour, R. J., Walborn, N. R., & Gull, T. R. 1986, ApJ, 305, 867
Drissen, L., Robert, C., Lamontagne, R., Moffat, A. F. J., St.-Louis, N., van Weeren, N., & van Genderen, A. M. 1989, ApJ, 343, 426
Dufour, R. J., Parker, R. A., & Henize, K. G. 1988, ApJ, 327, 859
Gallagher, J. S. 1989, in IAU Colloq. 113, Physics of Luminous Blue Variables, ed. K. Davidson, A. F. J. Moffat, & H. J. G. L. M. Lamers (Dordrecht: Kluwer), 185
Garmany, C. D., Conti, P. S., & Massey, P. 1980, ApJ, 242, 1063
Greenstein, N. K. 1938, Harvard Bull., 908, 25
Heinze, K. G. 1976, ApJS, 30, 491
Hester, J. J., Light, R. M., Westphal, J. A., Currie, D. G., Groth, E. J., Holtzman, J. A., Lauer, T. R., & O'Neil, E. J., Jr. 1991, AJ, 102, 654
Humphreys, R. M. 1989, in IAU Colloq. 113, Physics of Luminous Blue Variables, ed. K. Davidson, A. F. J. Mofat, & H. J. G. L. M. Lamers (Dordrecht: Kluwer), 3
———. 1991, in IAU Symp. 143, Wolf-Rayet Stars and Interrelations with Other Massive Stars in Galaxies, ed. K. A. van der Hucht & B. Hidayat (Dordrecht: Kluwer), 485
Humphreys, R. M., Lamers, H. J. G. L. M., Hoekzema, N., & Cassatella, A. 1989, A&A, 218, L17
Johnson, H. M. 1976, ApJ, 206, 469
———. 1980, ApJ, 235, 66
———. 1982, ApJ, 256, 559
Kenyon, S. J., & Gallagher, J. S. 1985, ApJ, 290, 542
Königl, A. 1982, ApJ, 261, 115
Lamers, H. J. G. L. M., & Fitzpatrick, E. L. 1988, ApJ, 324, 279
Langer, N., & El Eid, M. F. 1986, A&A, 167, 265
Leitherer, C. 1990, ApJS, 73, 1
Leitherer, C., Appenzeller, I., Klare, G., Lamers, H. J. G. L. M., Stahl, O., & Waters, L. B. F. M. 1985, A&A, 153, 168
Leitherer, C., & Chavarría, C. 1987, A&A, 175, 208
Maeder, A. 1989, in IAU Colloq. 113, Physics of Luminous Blue Variables, ed. K. Davidson, A. F. J. Moffat, & H. J. G. L. M. Lamers (Dordrecht: Kluwer), 15
———. 1990, A&AS, 84, 139
Mayall, M. W. 1969, JRASC, 63, 221
McGregor, P. J., Finlayson, K., Hyland, A. R., Joy, M., Harvey, P. M., & Lester, D. F. 1988, ApJ, 329, 874
Merrill, P. W., & Burwell, C. G. 1933, ApJ, 78, 87
Mitra, M. P., & Dufour, R. J. 1990, MNRAS, 242, 98
Münch, L. M., & Morgan, W. W. 1953, Bol. Obs. Tonantzintla y Tacubaya, 1, No. 8, 19
Nota, A., & Paresce, F. 1989, in IAU Colloq. 113, Physics of Luminous Blue Variables, ed. K. Davidson, A. F. J. Moffat, & H. J. G. L. M. Lamers (Dordrecht: Kluwer), 159

Oke, J. B. 1974, ApJS, 236, 21
Osterbrock, D. E. 1989, Astrophysics of Gaseous Nebulae and Active Galactic Nuclei (Mill Valley: University Science Books)
Paresce, F., Burrows, C., & Horne, K. 1988, ApJ, 329, 318
Paresce, F., & Nota, A. 1989, ApJ, 341, L83
Perek, L., & Kohoutek, L. 1967, Catalogue of Galactic Planetary Nebulae (Prague: Academia)
Pottasch, S. R. 1980, A&A, 89, 336
Raga, A. C., & Cantó, J. 1989, ApJ, 344, 404
Schulte-Ladbeck, R. E., Meade, M. R., & Hillier, D. J. 1992, in Nonisotropic and Variable Outflows from Stars, ed. L. Drissen, C. Leitherer, & A. Nota (ASP Conf. Ser. 22), 118
Smith, L. J. 1991 in IAU Symp. 143, Wolf-Rayet Stars and Interrelations with Other Massive Stars in Galaxies, ed. K. A. van der Hucht & B. Hidayat (Dordrecht: Kluwer), 385
Sreenivasan, S. R., & Wilson, W. J. F. 1989, in IAU Colloq. 113, Physics of Luminous Blue Variables, ed. K. Davidson, A. F. J. Moffat, & H. J. G. L. M. Lamers (Dordrecht: Kluwer), 205
Stahl, O. 1986, A&A, 164, 321
———. 1987, A&A, 182, 229
Stahl, O., Wolf, B., Klare, G., Cassatella, A., Krautter, J., Persi, P., & Ferrari-Toniolo, M. 1983, A&A, 127, 49
Stahl, O., Wolf, B., & Zickgraf, F.-J. 1987, A&A, 184, 193
Stencel, R., Pesce, J., & Bauer, W. 1988, AJ, 95, 141
Stone, R. P. S. 1977, ApJ, 218, 767
Taylor, M., Nordsieck, K. H., Schulte-Ladbeck, R. E., & Bjorkman, K. S. 1991, AJ, 102, 1197
Thackerary, A. D. 1950, MNRAS, 110, 526
Thackerary, A. D. 1956, Vistas Astron., 2, 1380
———. 1977, MNRAS, 180, 95
Viotti, R. 1971, PASP, 83, 170
Viotti, R., Altamore, A., Barylak, M., Cassatella, A., Gilmozzi, R., & Rossi, C. 1984, in Future of Ultraviolet Astronomy Based on Six Years of IUE Research (NASA CP-2349), ed. J. M. Mead, R. D. Chapman, & Y. Kondo, 231
Viotti, R., Cassatela, A., Ponz, D., & Thé, P. S. 1988, A&A, 190, 333
Walborn, N. R. 1989, in IAU Colloq. 108, Atmospheric Diagnostics of Stellar Evolution: Chemical Peculiarity, Mass Loss and Explosion, ed. K. Nomoto (Berlin: Springer-Verlag), 70
Walborn, N. R., & Blanco, B. M. 1988, PASP, 100, 797
Walborn, N. R., Blanco, B. M., & Thackeray, A. D. 1978, ApJ, 219, 498
Westerlund, B. E., & Henize, K. G. 1967, ApJS, 14, 154
White, R. L., & Becker, R. H. 1985, ApJ, 297, 677
Whitelock, P. A., Carter, P. S., Roberts, G., Whittet, D. C. B., & Baines, D. W. T. 1983, MNRAS, 205, 577
Whitford, A. E. 1958, AJ, 63, 201
Wisse, P. N. J., & Wisse, M. 1971, A&A, 12, 149
Wolf, B., & Stahl, O. 1982, A&A, 112, 111
Wood, H. E. 1914, MNRAS, 74, 698
Zickgraf, F. J. 1989, in IAU Colloq. 113, Physics of Luminous Blue Variables, ed. K. Davidson, A. F. J. Moffat, & H. J. G. L. M. Lamers (Dordrecht: Kluwer), 117
———. 1992, in Nonisotropic and Variable Outflows from Stars, ed. L. Drissen, C. Leitherer, & A. Nota (ASP Conf. Ser. 22), 75
Zickgraf, F. J., Wolf, B., Stahl, O., Leitherer, C., & Appenzeller, I. 1986, A&A, 163, 119